Book of Tutorials and Abstracts

European Microbeam Analysis Society

EMAS 2023

17th

EUROPEAN WORKSHOP

on

MODERN DEVELOPMENTS AND APPLICATIONS IN MICROBEAM ANALYSIS

7 to 11 May 2023
at the
Jagiellonian University, Auditorium Maximum
Krakow, Poland

Under the auspices of the Rector of the
Jagiellonian University, Krakow, Poland
Organised in collaboration with the
Institute of Metallurgy and Materials Science of
the Polish Academy of Sciences, Krakow, Poland

EMAS
European Microbeam Analysis Society eV
www.microbeamanalysis.eu/

This volume is published by:
European Microbeam Analysis Society eV (EMAS)
EMAS Secretariat
c/o Eidgenössische Technische Hochschule, Institut für Geochemie und Petrologie
Clausiusstrasse 25
8092 Zürich
Switzerland

ISBN 978 90 8227 6961
NUR code: 972 – Materials Science

EXPLORING THE LIMITS OF LOW VOLTAGE EPMA OF COATED SAMPLES

Michael B. Matthews

AWE Plc.
Aldermaston, Reading RG7 4PR, Great Britain
e-mail: matthm@hotmail.com

Mike has been operating EPMA for over 30 years, starting with a Cameca Camebax Microbeam analysing mantle garnets at the University of Edinburgh in 1987. From Edinburgh he spent a year setting up and running the EPMA facility for Anamet Services, the analysis arm of Rio Tinto Zinc, in their labs near Bristol, then moving on to Johnson Matthey's Technology Centre in Reading for the next 13 years, analysing platinum group metal products, including autocatalysts and fuel cells. More recently, he completed a PhD on EPMA analysis of radioactive materials as a mature student at the University of Bristol, sponsored by his current employer, AWE Plc. He is currently the President of the International Union of Microbeam Analysis Societies (IUMAS), Chair of the UK representation on the International Standards Technical Committee on Microbeam Analysis, ISO/TC202, and is a former President of the European Microbeam Analysis Society (EMAS).

1. *A MICRO-GUIDE TO MICRO-ANALYSIS*

In order to appreciate the strengths and limits of electron probe microanalysis (EPMA) of or through thin coatings on materials it is necessary to have at least a basic understanding of how an EPMA operates. Here we present only a very simplistic explanation of the necessary factors and mechanisms. Readers interested in a more complete understanding of EPMA as an analysis method are directed to more detailed and inclusive texts, such as Reed [1]; Hren *et al.*[2]; Goldstein *et al.* [3]; and Llovet *et al.* [4].

Using a high voltage and electro-magnetic lenses, a beam of electrons is accelerated and focussed into a sub-micrometre spot on the sample surface (Fig. 1a). The electrons enter the sample, scattering and losing energy as they interact with its atoms (Fig. 1b).

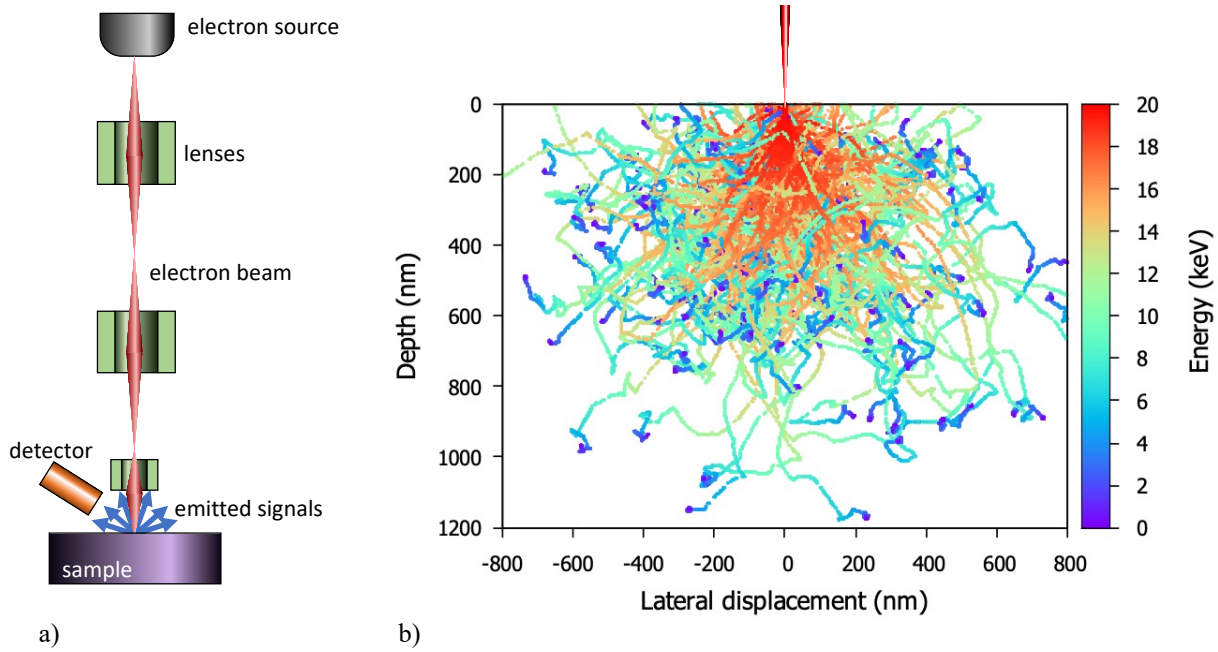

Figure 1. Schematics of a) an EPMA, and b) electron scattering and energy loss in the sample [5].

The combination of scatter and energy loss produces a roughly hemispherical electron interaction volume of the order of ~ 1 µm diameter. The absolute size is a function of the mean atomic number of the sample, with higher Z materials slowing the electrons more rapidly, and of the accelerating voltage, with lower voltages imparting less kinetic energy to the beam of electrons so they come to rest after fewer interactions in the sample. Figure 2 compares the electron interaction volumes in a pure Fe sample at two different beam energies. At 20 kV, which can be considered to be a 'normal' analysis condition (typically in the range 15 - 25 kV), the electron interaction volume is approximately 1 µm diameter and depth. For a 'low voltage' analysis condition of 10 kV this reduces to ~ 350 nm.

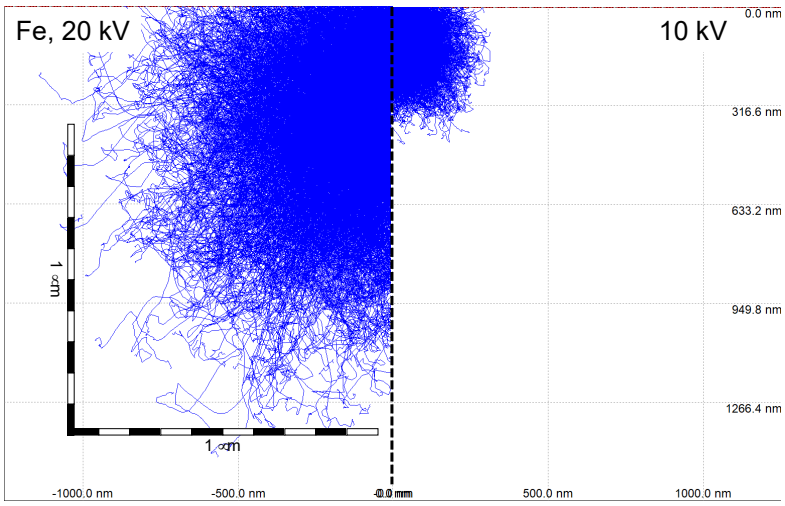

Figure 2. Comparison of electron interaction volumes in a pure Fe sample for a 20 kV electron beam (left half) and a 10 kV beam (right half). Modelled using CASINO [6].

If an electron has sufficient kinetic energy, measured in electron volts (eV), an interaction with a sample atom may knock out one of its inner shell electrons. To fill the resulting gap the atom's electron occupancy an outer shell electron can cascade down. To do this it has to lose the energy difference between the two shells, for example by emitting an X-ray with an energy equal to the inter-shell energy difference. Since the number and magnitude of electron energy levels are determined by the number of protons in the atom's nucleus, the possible inter-shell transitions are characteristic to each element. Thus, by measuring the spectrum of X-rays emitted from a sample we can determine what elements are present within the micron-scale interaction volume being 'probed' by our electron beam.

Figure 3a shows a Bohr-Rutherford model of an atom, where the electron energies are represented as concentric rings. In this example there are three 'shells': K, L and M. The K-shell, the inner-most in all atoms, has a single energy level but the L-shell has three sub-shells, L1 to L3, whilst the M-shell has five sub-shells. The number of sub-shells increases by two with every successive shell series an atom has. Ionisation can occur in any sub-shell and relaxation can occur from (almost) any sub-shell with a higher energy but each combination has an associated probability for a given element. Figure 3b shows an example measured X-ray spectrum for a pure Fe sample with three characteristic X-ray peaks.

If we account for several correction factors, such as the probability of a given shell ionisation and relaxation combination occurring, the rate of deceleration of the electrons in the sample, and the probability that a generated X-ray will exit the sample surface and reach our detector, we can convert the number of detected X-rays from each element into a quantitative analysis of that micrometre-scale volume.

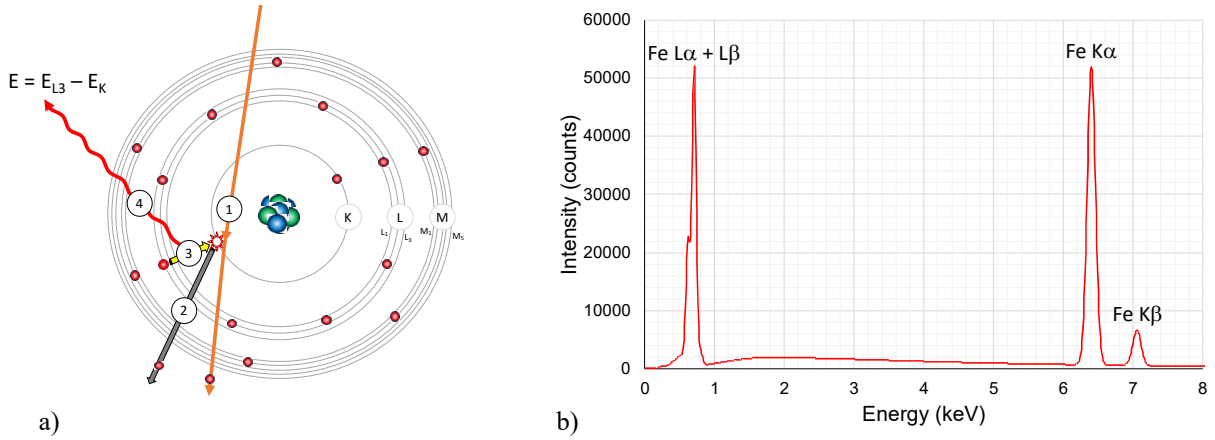

Figure 3. a) Bohr-Rutherford model of an atom illustrating the generation of a characteristic energy X-ray as a result of an inner-shell ionisation, and b) an example X-ray spectrum showing the resulting characteristic X-ray lines from a pure Fe sample analysed at 20 kV.

One of the functions we need to understand to carry out any form of quantitative analysis is the depth distribution function of a given characteristic X-ray generated in the sample. Called the $\phi\rho(z)$-curve, this typically has a finite value at the sample surface, termed the ϕ_0-value, increases to a maximum below the sample surface then tails off to zero at the maximum depth of X-ray generation. Paired with the generated $\phi(\rho z)$-curve is the emitted $\phi(\rho z)$-curve. This takes into account the proportion of the generated X-rays that are absorbed before they reach the surface. Figure 4 shows both sets of curves for both Kα and Lα X-ray lines for a pure Fe sample. The Lα X-ray line, with a critical excitation energy (the minimum energy needed to cause the ionisation), E_c, of 0.707 keV can be generated by lower energy electrons and are therefore generated to a greater depth than the Kα X-ray line with a critical excitation energy of 7.110 keV. The resulting Lα X-ray at 0.704 keV has a much higher probability of being absorbed than the Kα X-ray at 6.400 keV so its emitted $\phi(\rho z)$-curve is much reduced compared to its generated curve. Thus, whilst the Lα-line has a higher probability of being generated the emitted intensities in this example are very similar for both lines. This is reflected in the Lα- and Kα-peaks being almost the same size in Fig. 4b.

2. *THE EFFECT OF SURFACE COATING*

In order to ensure good electrical conductivity of our sample we typically coat it with a thin (10 - 20 nm) of conductive material such as carbon. Figure 5a shows that, under 'normal' analysis conditions such a coating produces very little difference in the emitted X-ray intensities compared to an uncoated sample, even for the relatively low energy Fe Lα-line in this example. At low accelerating voltages, as we saw above, the electron interaction volume is significantly

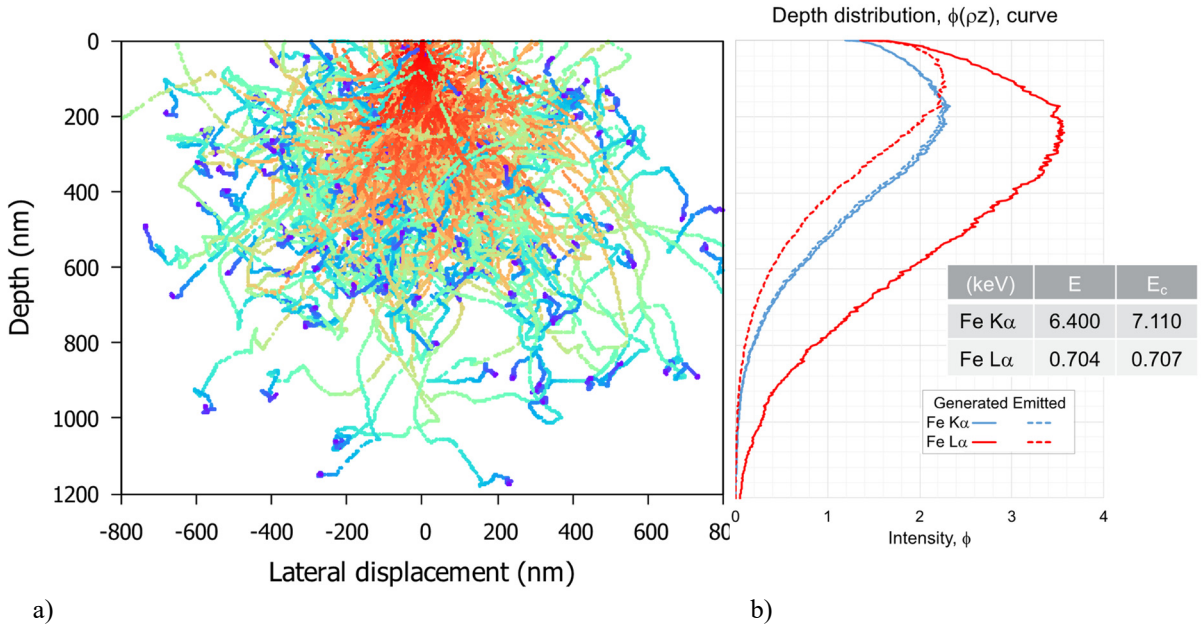

Figure 4. a) Electron energy scatter plot for a 20 kV electron beam in a pure Fe sample, and b) generated and emitted X-ray depth distribution curves calculated for the same sample and conditions. The lower energy Lα X-rays are generated to a greater depth but suffer proportionally more absorption than the higher energy Kα X-rays.

reduced and, as Fig. 5b shows, our 15 nm 'thin' C-coating now represents a significant proportion of the interaction volume and now has a measurable effect on the emitted X-ray intensities from the sample.

For a given coating-substrate model, we can calculate the magnitude of this effect over ranges of coating thicknesses and accelerating voltages. Figure 6 shows the curves for both Fe Lα and C Kα calculated for the model in Fig. 5, with C coating thicknesses of 5 - 20 nm at accelerating voltages of 3 - 20 kV. The plotted k-ratios values are the intensities calculated for the coated sample relative to those for an uncoated reference so directly give the proportion effect of the C-coating at each condition. Above ~ 15 kV the coating has very little effect on the sample intensities and it is even difficult to detect the presence of the coating from C Kα measurements. As the accelerating voltage is reduced, the effect is initially small but increases rapidly. At 5 kV a 20 nm C coating reduces the emitted Fe Lα intensity by 10 %. At 3 kV the same coating absorbs 45 % of the Fe Lα X-rays.

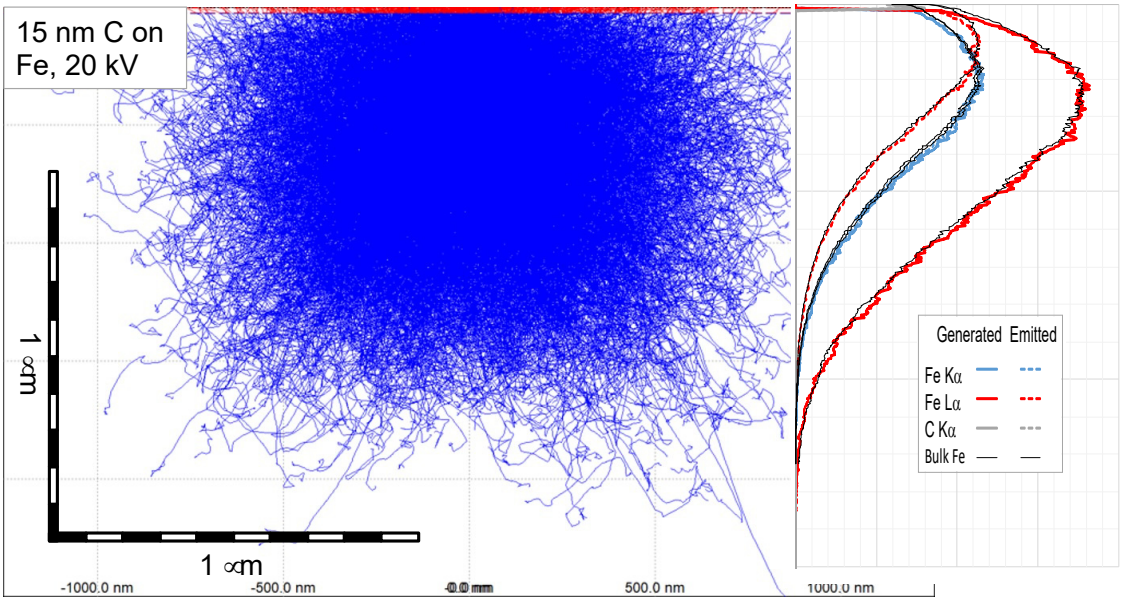

a)

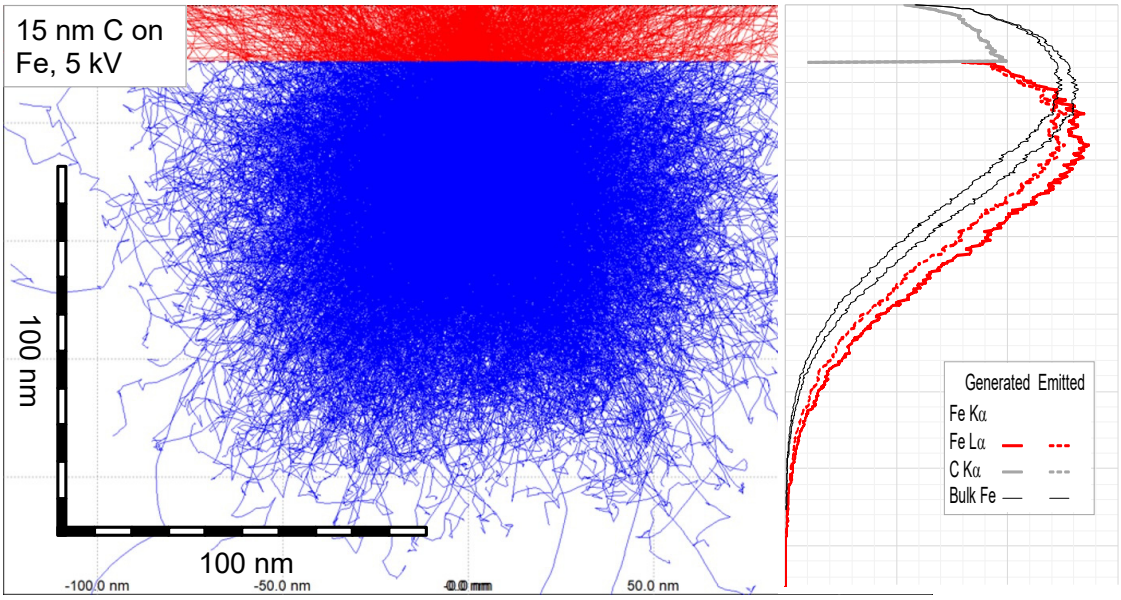

b)

Figure 5. Comparison of the relative effects of a 15 nm C-coating on a pure Fe sample at a) 20 kV, and b) 5 kV. The red region in each scatter plot shows the relative size and position of the C-coating. The black traces in the $\phi(\rho z)$-plots give the depth distribution curves for an uncoated sample to compare against those for the coated samples.

Figure 6 also shows that not only does the impact of the coating become rapidly greater at low accelerating voltages, its thickness also has a proportionally greater impact. Thus, whilst we may be able to ignore the presence of the coating at normal accelerating voltages, at low voltages it becomes increasingly important to accurately know thick it is.

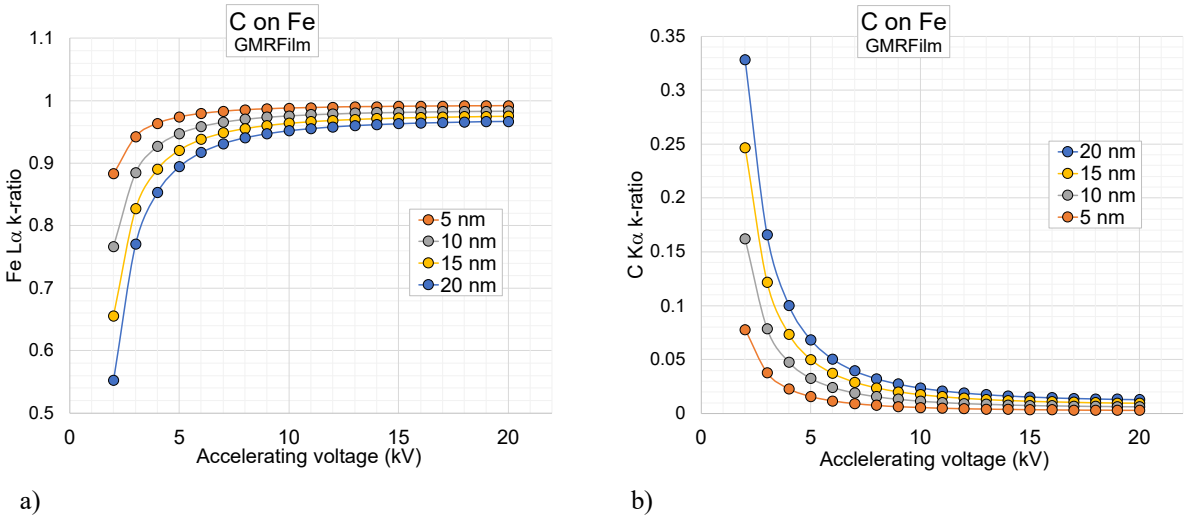

Figure 6. Calculated relative emitted intensity curves for a) Fe Lα and b) C Kα for C coated pure Fe samples. The *k*-ratio values plotted are the emitted intensities of the coated sample at each condition relative to an uncoated reference at the same accelerating voltage.

3. SOFTWARE TOOLS

Many of the diagrams above, for example the electron scattering plots, have been generated using readily available software. There are several options available, some entirely free for academic use. They can be divided into 2 main types, direct calculation and Monte Carlo modelling.

The first type uses the same correction routines as are used for bulk analysis in an EPMA but modified to include some sample geometry, such as a surface coating layer. These can be directly used to either calculate the emitted intensities for a theoretical model or to calculate coating thickness and/or composition and/or substrate composition from measured X-ray intensities. Examples of this include GMRFILM [7] and BADGERFILM [8-10].

The Monte Carlo method simulates individual electron tracks in a sample model. Each track is modelled step-by-step as a series of short path lengths. At each step, a range of possible interaction events can take place, for example scattering or energy loss, each with its own probability of occurring. A random number generator is used to model whether a given event occurs and what its effect on the electron is. The next step is then modelled with any modified energy and/or direction of the electron. This is akin to rolling dice to gamble on whether or not an event occurs at each step, hence the name Monte Carlo. Any secondary signals, such as an X-ray emission, also are modelled. The more trajectories that are randomly modelled in this way the more statistically precise the output results are. In practice, this requires tens or hundreds of thousands of tracks to be modelled to produce useful values. The main benefit of this approach is that very complex sample models can be calculated. The drawbacks are: They are slower than

the direct calculation method, ranging from tens of seconds to tens of hours; they cannot be directly used to calculate sample compositions from measured intensities. Examples include CASINO [6], DTSA-II [11] and PENEPMA [12].

4. REAL WORLD APPLICATION - PLUTONIUM OXIDE THICKNESSES

Although Pu is the metal that you're least likely to ever encounter it does oxidise very readily in air and can grow a relatively thick oxide before spalling off. Additionally, Stanford *et al.* [13] recently produced a very useful dataset of EPMA analyses combined with focussed ion beam (FIB) cross-sections through a large number of Pu oxide thicknesses, ranging from ~ 30 nm up to 400 nm. The FIB cross-sections provided direct measurements of the true thicknesses and allowed them to correlate the EPMA measured O Kα k-ratios (relative to a bulk PuO_2 reference) as functions of the oxide thickness (Fig. 7). Their aim was to create a calibration curve to be able to directly determine oxide thickness from measured O *k*-ratios but we can use their data to test the software tools.

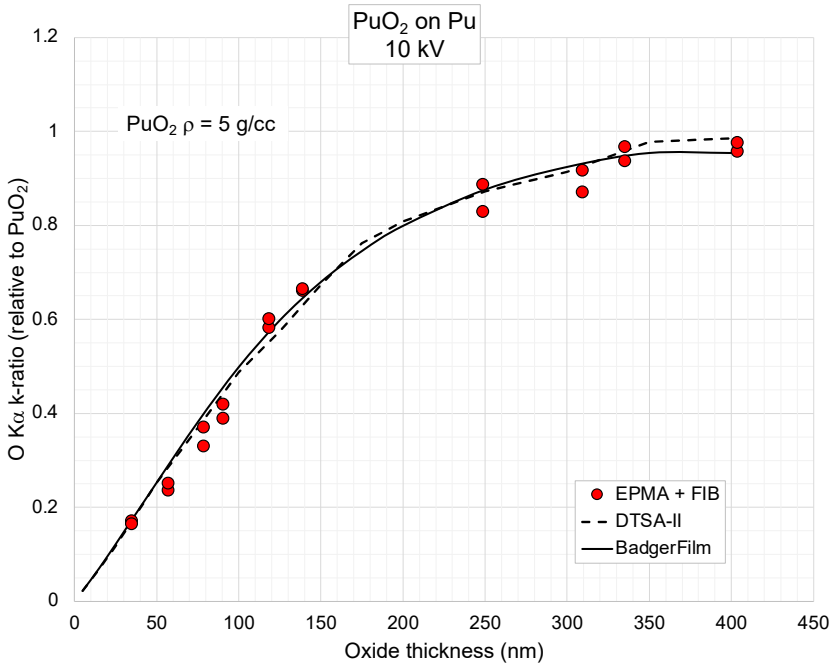

Figure 7. Modelling the Stanford et al data to calculated PuO_2 thickness versus O Kα *k*-ratio values using DTSA-II and BADGERFILM.

Figure 7 shows the EPMA + FIB experimental data acquired at 10 kV and thickness versus *k*-ratio curves calculated using DTSA-II, a Monte Carlo programme, and BADGERFILM, a direct calculation programme. The two software tools produce very similar results and are both able to match the experimental data with reasonable accuracy over the full thickness range.

5. *A USEFUL SHORTCUT*

The experimental data in Fig. 7 covers a very wide range of thicknesses. In practice, we frequently have at least some concept of the thickness range we are interested in measuring. For example, applied conductive coatings for EPMA analysis are commonly in the range of 10 – 20 nm. We also have the benefit of knowing the composition of the coating even if we have little foreknowledge of the sample chemistry. Looking at the modelled profiles in Fig. 7 the first 100 nm of oxide is very close to a straight-line relationship. In fact, if we choose a sufficiently small range of thicknesses any part of the curve can be very closely approximated by straight-line segments.

Figure 8 shows an example set of data calculated for a C coated pure Fe sample. *k*-ratios were calculated using GMRFILM [7] for coating thicknesses of 5, 10, 15 and 20 nm, at accelerating voltages of 5, 7, 10, 15 and 20 kV. At each accelerating voltage the four thickness versus *k*-ratio data points for each X-ray line lie very close to a straight-line, indicated by the dashed lines in the figures, with R^2 fit values of better than 0.9995 even at 5 kV. The plots show that, not only can the coating thickness versus C Kα *k*-ratio relationship be very closely approximated by a straight-line function, but the substrate *k*-ratio is also very close to linear.

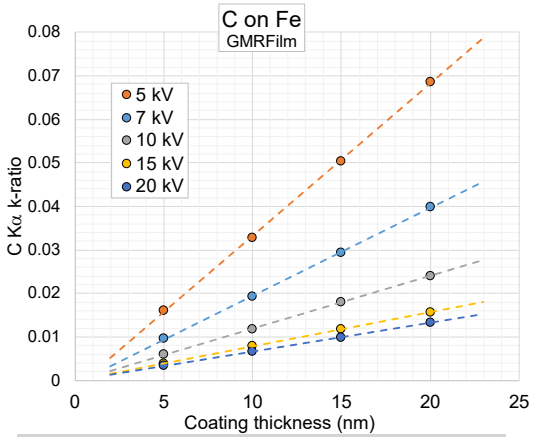

	C Kα		
kV	m	c	R^2
5	0.00351	-0.00193	0.99970
7	0.00202	-0.00081	0.99982
10	0.00121	-0.00031	0.99992
15	0.00079	-0.00010	0.99998
20	0.00066	-0.00005	0.99999

a)

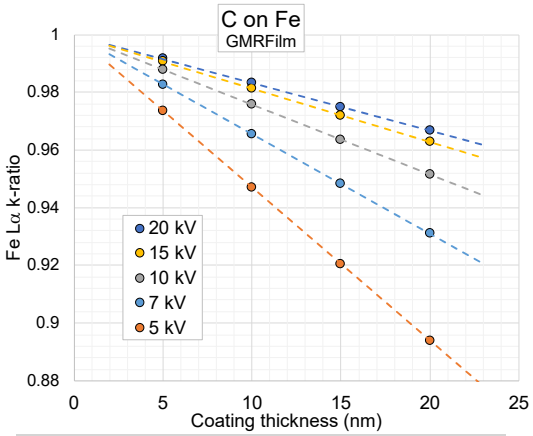

	Fe Lα		
kV	m	c	R^2
5	-0.00531	1.00025	1.00000
7	-0.00345	1.00003	1.00000
10	-0.00241	0.99991	1.00000
15	-0.00185	0.99988	1.00000
20	-0.00165	0.99988	0.99999

b)

Figure 8. Modelled coating thickness versus a) C Kα *k*-ratio and b) Fe Lα *k*-ratio values for a C-coating on a pure Fe substrate. The dashed lines are linear fits through each of the datasets, with the corresponding linear parameters, *m* and *c*, and R^2 fit factors given in the tables below each plot.

If we plot the linear parameter values for both the coating and the substrate as functions of accelerating voltage, as shown in Fig. 9, the values vary smoothly with voltage. We can therefore calculate models at a few voltages and interpolate for intermediary voltages as required.

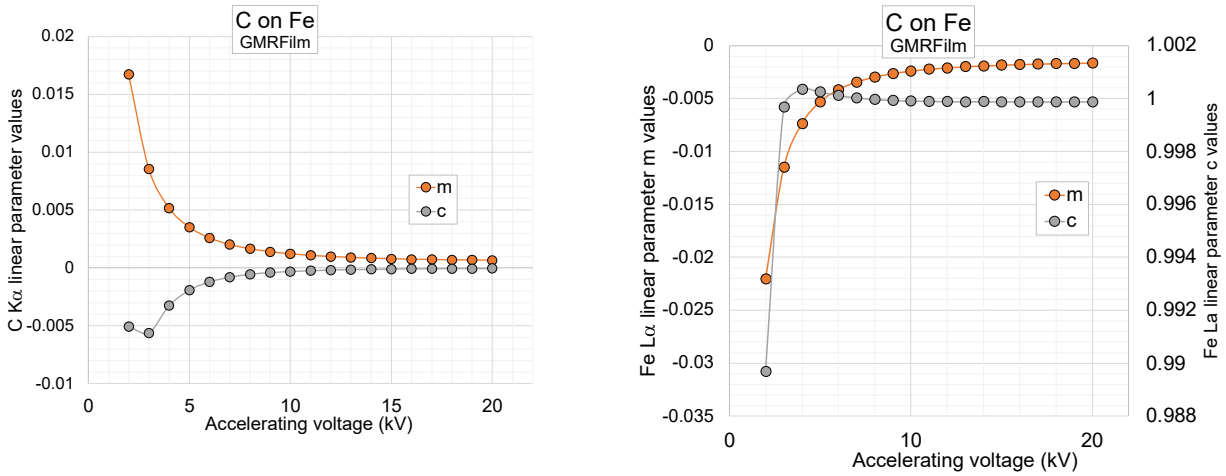

a) b)

Figure 9. Plots of a) C Kα, and b) Fe Lα linear parameter values as functions of accelerating voltage for the C on Fe model in Figure 8.

The coating linear parameter values are not independent of the composition of the substrate so we cannot use a single set of coating calculations for all samples. As Fig. 10 shows, the change in both the gradient, *m*, and intercept, *c*, vary gradually and smoothly with substrate mean atomic number, Z. Thus, even if we have very little foreknowledge of the substrate, if we can estimate its mean atomic number, we can still predict the linear parameter values with some level of confidence.

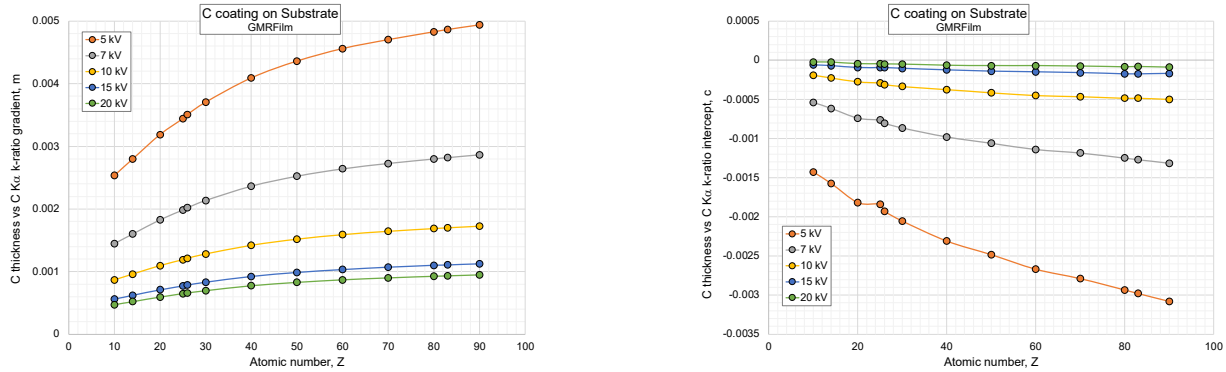

a) b)

Figure 10. Plots of variation of the linear parameter a) gradient, *m*, and b) intercept, *c*, for a C-coating on a substrate with mean atomic number Z.

This linear parameterisation method is particularly useful if we have large datasets of measurements that need measuring and/or correcting for the coating thickness. Pre-calculation of the model incurs some initial time overhead, but once this is done and the linear parameter values determined, we can very quickly calculate coating thicknesses for any number of data points. The linear parameter values are also instrument-independent so can be re-used on different instruments or in different labs.

If we have enough foreknowledge of the sample to model, it is chemistry we can then use the calculated coating thickness to apply a correction to the measured substrate *k*-ratio(s) to correct for the effect of the coating to effectively carry out an uncoated sample analysis.

6. COATING ACCURACY AND SUBSTRATE QUANTIFICATION

As was shown in Fig. 6, as we work at lower accelerating voltages, we need to know the thickness of our coatings with greater accuracy. Many coaters have built in film thickness monitoring (FTM) systems that allow us to control the thickness of coating deposition in real time. There are two main configurations of coater-FTM combinations. The most common configuration sites the FTM to one side of the sample platen, but systems are available with the FTM co-located with the samples being coated. Both configurations are shown schematically in Fig. 11. The FTM measures the coating being deposited on the sensor. A 'tooling factor' correction is applied to compensate for any difference in distance of the sensor from the coating source compared to the sample distance from the source.

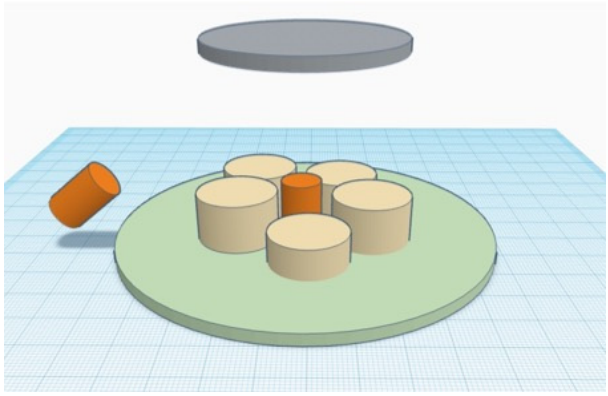

Figure 11. Schematic of a sputter coater showing the two FTM configurations, shown by the orange cylinders; either to one side of the sample platen (green disk) or co-located with the samples (tan cylinders). The grey disk is the sputter source.

6.1. Cu on Bi, Co-located FTM

Four polished Bi samples were coated with Cu to FTM measured thicknesses of ~ 5, 10, 15 and 20 nm in a sputter coater where the FTM sensor was co-located with the samples. In order to test the repeatability of the coating deposition the FTM was set to deposit a nominal thickness of 5 nm and the thicker coatings were made by repeated depositions of 5 nm. Coating thicknesses were calculated from EPMA measured Cu Lα *k*-ratios using GMRFILM [7], DTSA-II [11] and PENEPMA [12]. For the 20 nm sample, the coating thickness was also measured directly from a FIB milled cross-section.

Figure 12a shows the resulting calculated and measured thicknesses. The three sets of values calculated from the EPMA measured Cu Lα *k*-ratios using DTSA-II, GMRFILM and PENEPMA all agree very closely with each other, and also with the directly measured thickness from the FIB section on the 20 nm sample. All these thicknesses are noticeably higher than the FTM measured values, with the relative difference ranging from ~ 10 % for the thickest coating to ~ 20 % for the thinnest (Fig. 12b).

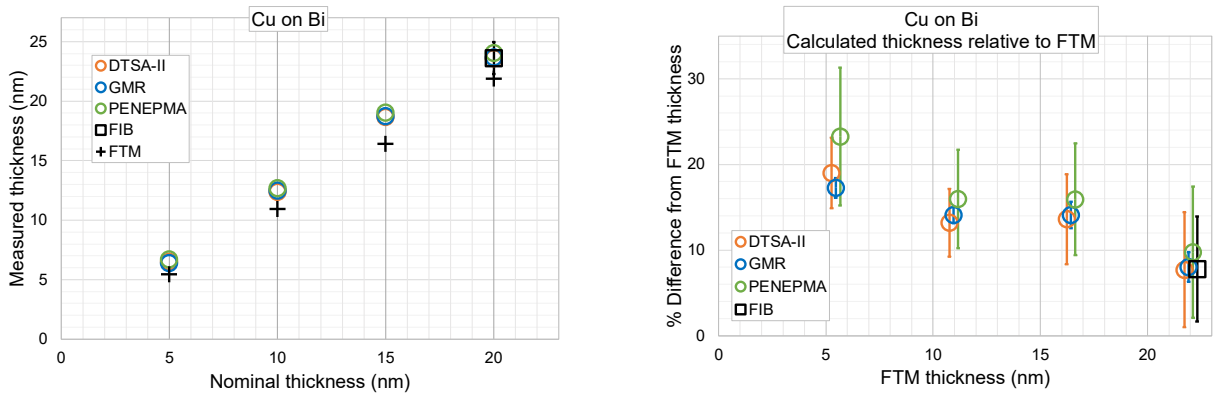

a) b)

Figure 12. a) Plot of the calculated and measured coating thicknesses of the four Cu coated Bi samples, and b) the percentage difference of the calculated and FIB measured thicknesses relative to the FTM values.

It is reassuring to note that all the datasets lie on straight lines. As stated above, each coating was deposited as 1 or more depositions of a set 5 nm target thickness. The straight-line trends thus show that the FTM controlled thickness is at least consistently repeatable.

What effect does a 10 - 20 % difference in assumed thickness have on the substrate quantification? We can use the same software packages we used to measure the coating thicknesses to calculate the Bi Mα *k*-ratio we would expect from the pure Bi substrate and compare those values against the EPMA measured *k*-ratios, giving us a direct determination of the substrate quantification error.

Figure 13a shows the resulting predicted *k*-ratios plotted against those measured directly on the EPMA for the thickest coated sample. Since we have several different thicknesses determined for each sample (i.e., from the FTM, from the FIB cross-section and calculated from EPMA measured Cu Lα *k*-ratios) we have three sets of calculated curves. For each set the Bi Mα *k*-ratio has been calculated using each of the three software models; PENEPMA, DTSA-II and GMRFILM. Note that, for the 'EPMA' set of curves, the PENEPMA calculated coating thickness values were used for the PENEPMA calculation of the Bi Mα *k*-ratios, and DTSA-II used for the DTSA-II curve, etc. The agreement looks reasonably good and at least predicts the trend in the substrate k-ratio as a function of accelerating voltage.

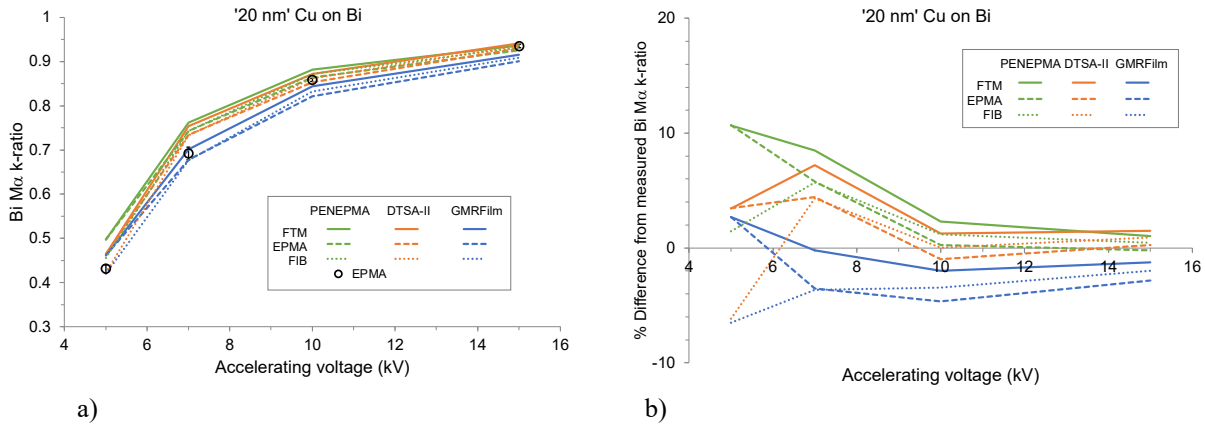

Figure 13 Calculated Bi Mα *k*-ratios plotted as a) absolute values, and b) as percent difference from Bi Mα *k*-ratios measured directly on the EPMA. Values are shown using coating thicknesses derived from the FTM and the FIB or calculated from EPMA measured Cu Lα *k*-ratios using PENEPMA, DTSA-II or GMRFILM.

Plotting the same data as a percentage difference from the EPMA directly measured *k*-ratios (Fig. 13b) i.e., the percentage error, the difference increases from better than ± 4 % at 15 kV to ± 10 % at 5 kV.

Note that no one set of data give the smallest error at all voltages: The PENEPMA predicted Bi Mα *k*-ratio using the EPMA + PENEPMA determined coating thickness gives the smallest error at 10 and 15 kV (the green dashed line in Fig. 13b) but performs poorer than many of the other models at the lower voltages for this model. Thus, we cannot use a 'high fidelity' Monte Carlo algorithm and claim that this gives us better answers.

6.2. Al on Bi, Side-located FTM

The Cu on Bi samples demonstrate what error magnitudes we can expect from well-behaved samples but much larger errors are also possible.

A similar set of experiments was carried out with Al deposited onto the polished Bi samples using a sputter coater with an FTM located to one side of the sample platen. Coating thicknesses were calculated as for the Cu on Bi samples above. Whilst the calculated thicknesses again all agree well with each other, the discrepancy with the FTM measurements (Fig. 14a) is far greater in this example, with relative errors of ~ 150 % (Fig. 14b) indicating that the side-mounted FTM sensor is introducing an appreciable error.

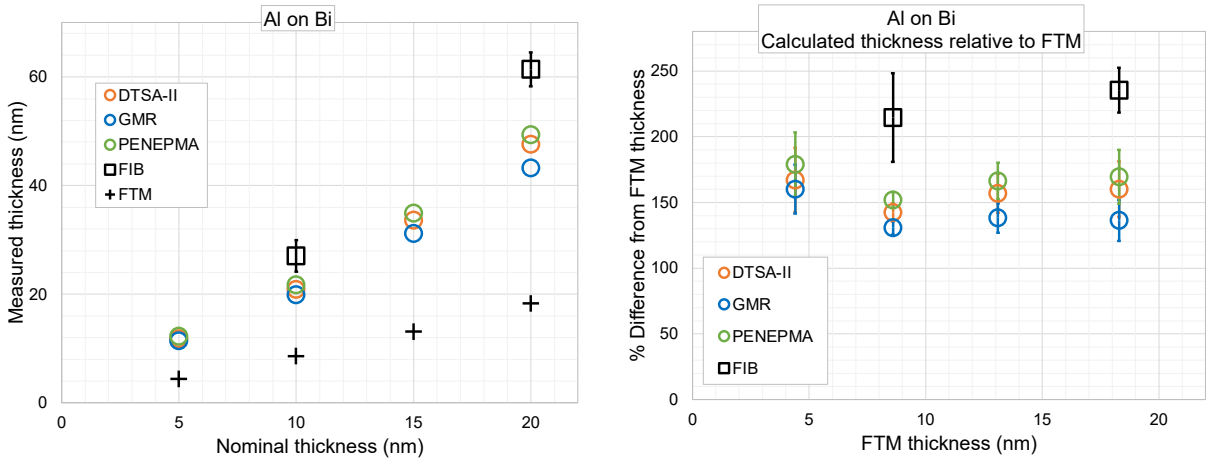

a) b)

Figure 14. a) Plot of the calculated and measured coating thicknesses of the four Al coated Bi samples, and b) the percentage difference of the calculated and FIB measured thicknesses relative to the FTM values.

There is also a very clear mismatch between the calculated thicknesses and the two FIB measured values. Since the FIB values are a direct measure of the geometric thickness whilst the calculated thicknesses are a function of the assumed layer density, we can imply that the discrepancy is due to an incorrect density value being used.

Several studies have shown that thin film densities can be lower than for bulk materials [14-22].` Hartman [16] reported vacuum evaporated Al film densities increasing slowly from ~ 2.5 g/cm^3 for a 60 nm film to ~ 2.6 g/cm^3 for a 200 nm film, compared to a bulk Al density of 2.7 g/cm^3 (Fig. 15). Below 50 nm, the density drops rapidly, reaching a value of only 2.0 g/cm^3 for a 25 nm film, the thinnest he reported. Using this lowest value and recalculating the film thickness measurements brings these values into good agreement with the FIB values (Fig. 16a) but increases the discrepancy with the FTM values to a very substantial 250 % relative difference (Fig. 16b).

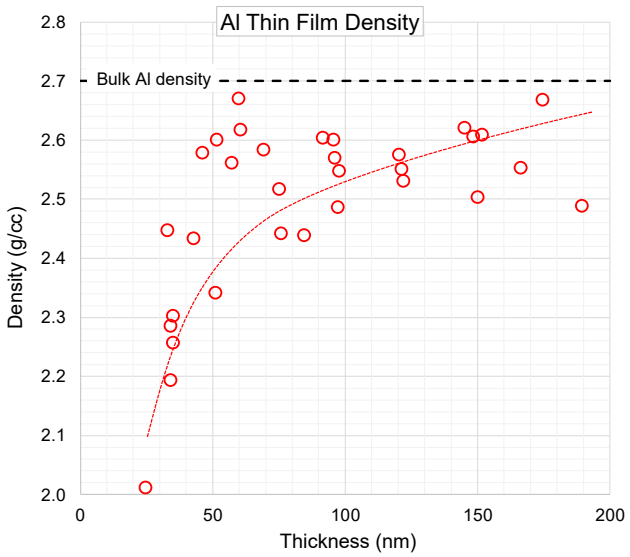

Figure 15. Density as a function of Al film thickness data from Hartman [16]. The red dashed line is hand-drawn to indicate the general trend of the data. The black dashed line shows the density of bulk Al.

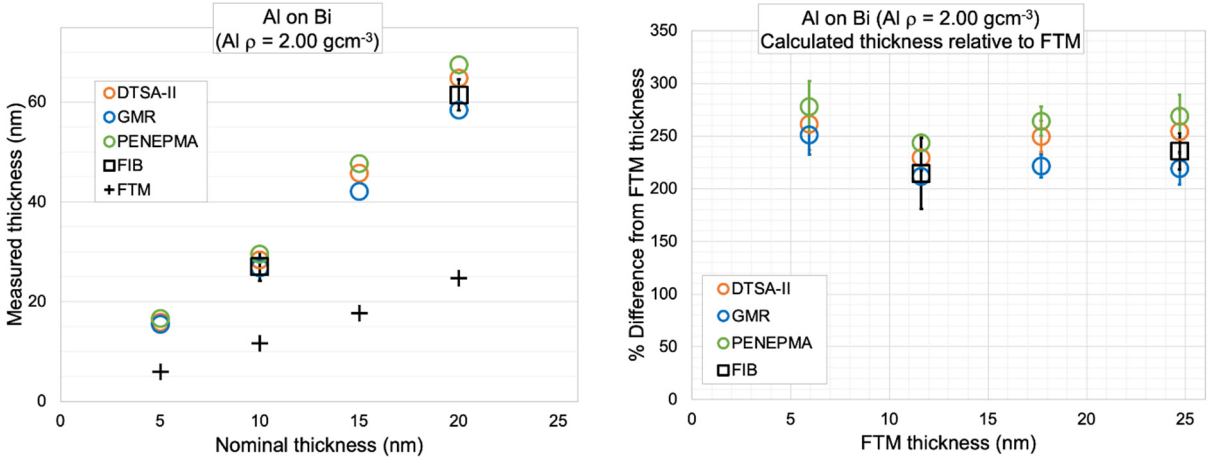

a) b)

Figure 16. a) Plot of the re-calculated and measured coating thicknesses of the four Al coated Bi samples, and b) the percentage difference of the re-calculated and FIB measured thicknesses relative to the FTM values using an Al density value of 2.0 g/cm^3.

This level of disagreement is obviously expected to have a significant impact on quantification of the substrate, and this is borne out in Fig. 17. This shows the Bi Mα *k*-ratios for the '20 nm Al on Bi sample' both as the absolute calculated Bi Mα *k*-ratios compared to the measured values (Fig. 17a), and as the difference between the calculated *k*-ratios relative to the EPMA measurements (Fig. 17b). The values calculated using the FTM measured Al thicknesses (shown

as the solid lines in both plots) show errors increasing to 60 - 70 % at 5 kV. However, even using the EPMA calculated values produces errors of 20 - 40 % at 5kV, indicating that even with 'good' coating thickness measurements, errors can be substantial at lower accelerating voltages.

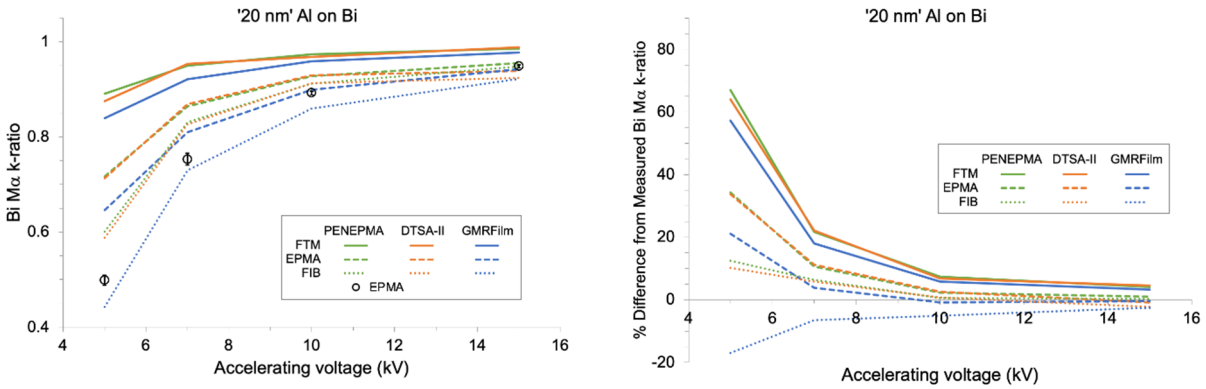

a) b)

Figure 17. Calculated Bi Mα *k*-ratios plotted as a) absolute values, and b) as percent difference from Bi Mα *k*-ratios measured directly on the EPMA. Values are shown using coating thicknesses derived from the FTM and the FIB or calculated from EPMA measured Al Kα *k*-ratios using PENEPMA, DTSA-II or GMRFILm using an Al density of 2.0 g/cm^3.

7. *DISCUSSION*

The increase in substrate quantification error with decreasing voltage is at least in part to be expected: As the voltage decreases the proportion of the analysis volume reaching the substrate decreases and consequently the substrate *k*-ratio also decreases. Any systematic errors in the models thus become proportionally larger relative to these smaller *k*-ratios.

There are almost certainly other factors also at play: For example, as the maximum analysis depth decreases at lower voltages the modelling of the emission intensities at the sample surface, ϕ_0, becomes more critical. Similarly, a larger portion of the imparted energy in this region (and therefore how much is available to generate X-rays) is more strongly influenced by how much is lost via backscattered electrons so accurate knowledge of the backscatter coefficients becomes more important. These factors will affect both coating and substrate quantifications.

Regardless of the mechanisms, the increase in error can be expected for all coating/substrate combinations and large potential errors need to be anticipated when analysing at low voltages: At 5kV, errors of ± 10 % just from modelling inaccuracies will not be unusual.

A very significant source of the error is relying on the FTM thickness values from a coater with the FTM sensor not co-located with the samples, as is shown by the Al on Bi samples above. The large errors here have been attributed to the difference in coating distance between the samples and the FTM sensor [23]: The rate of deposition per unit area will decrease as a function of the square of the distance from the coating source. Thus, a surface 2 units from the source will only receive a quarter of the coating per unit time as 1 unit from the source. In systems where the FTM sensor is not co-located with the samples a correction factor is used to correct for this effect. If this factor is not carefully calibrated large errors can result. This is particularly true for small desktop coaters where the coating distances are short and even small differences in positions can produce proportionally large changes in relative distance.

Numerous studies (see the reference listed above) have shown that the density of thin films can be lower than for bulk materials. As the Al on Bi results above show, where the FTM thicknesses are compared against density-independent methods (such as FIB cross-sectioning) this can result in large discrepancies. Fortunately, for microanalysis the algorithms we use to calculate the effects of thin coatings also use the density of the coating material. So long as the same value is used for the FTM settings as for the microanalysis calculations, the effects cancel out.

8. KEY TAKE-HOME POINTS

There are 3 main points to take away from this presentation:

1. Quantification errors can and will increase with decreasing analysis voltages. Below ~ 10 kV the rate of increase rises rapidly. Errors of ± 10 % are not exceptional.
2. Do not trust the thicknesses quoted by your film thickness monitors, especially if the FTM sensor is not co-located with the samples. Whilst the coatings are probably repeatable (assuming the sensor and sample positions are not changed) do not be fooled by the Ångstrom-level precision quoted by the thickness monitor, it could be accurate to only ± 100 %!
3. The density of thin coatings can be significantly lower than bulk density. If it is important to know the 'true' thickness, this needs to be accounted for.

9. REFERENCES

[1] Reed S J B 1975 *Electron microprobe analysis*. [Cambridge: Cambridge University Press]

[2] Hren J J, Goldstein J I and Joy D C 1979 *Introduction to analytical electron microscopy*. (Hren J J, Goldstein J I and Joy D C; Eds.) [New York: Plenum Press]

[3] Goldstein J I, Newbury D E, Echlin P, Joy D C, Romig Jr. A D, Lyman C E, Fiori C and Lifshin E 1992 *Scanning electron microscopy and X-ray microanalysis. 2nd edition.* [New York: Plenum Press]

[4] Llovet X, Moy A, Pinard P T and Fournelle J H 2020 *Progr. Mater. Sci.* **114** 100673
[5] Matthews M B 2020 *Field emission gun electron probe microanalysis of radioactive materials*. PHD thesis. [Bristol, UK: University of Bristol]
[6] Drouin D, Couture A R, Joly D, Tastet X, Aimez V and Gauvin R 2007 *Scanning* **29** 92-101
[7] Waldo R A 1988 An iteration procedure to calculate film compositions and thicknesses in electron-probe microanalysis. in: *Microbeam analysis*. (Newbury D E; Ed.) [San Francisco: San Francisco Press] 310-314
[8] Moy A and Fournelle J 2021 *Microsc. Microanal.* **27** 266-283
[9] Moy A and Fournelle J 2021 *Microsc. Microanal.* **27** 284-296
[10] Moy A and Fournelle J J 2023 BadgerFilm: A new thin film analysis programme (with other useful applications) for EPMA. in: *Book of Tutorials and Abstracts of the EMAS 2023 Workshop*. [Zürich, Switzerland: European Microbeam Analysis Society eV (EMAS)]
[11] Ritchie N W M, Davis J and Newbury D E 2008 *Microsc. Microanal.* **14** (Suppl. S2) 1176-1177
[12] Lllovet X and Salvat F 2016 *IOP Conf. Ser.: Mater. Sci. Engng.* **109** 012009
[13] Stanford J A, Teslich N, Donald S, Saw C K, Gollott R and Dinh L N 2020 *J. Nucl. Mater.* **530** 151968
[14] Blois M S and Rieser L M 1954 *J. Appl. Phys.* **25** 338-340
[15] Leder L B and Suddeth J A 1960 *J. Appl. Phys. 31* 1422-1426
[16] Hartman T E 1965 *J. Vacuum Sci. Technol.* **2** 239
[17] Lovell S and Rollinson E 1968 *Nature* **218** 1179-1180
[18] Kerrick D M, Eminhizer L B and Villaume J F 1973 *Amer. Mineralogist* **58** 920-925
[19] Jurek K, Renner O and Krouský E 1994 *Mikrochimica Acta* **114-115** 323-326
[20] Bastin G F and Heijligers H J M 2000 *X-ray Spectrom.* **29** 212-238
[21] Campos C S, Coleoni E A, Trincavelli J C, Kaschny J, Hubbler R, Soares M R F and Vasconcellos M A Z 2001 *X-ray Spectrom.* **30** 253-259
[22] Campos C S, Vasconcellos M A Z, Llovet X and Salvat F 2004 Microchimica Acta **145** 13-17
[23] Matthews M B, Kearns S L and Buse B 2018 *Microsc. Microanal.* **24** 83-92